Int. J. Solids Structures, 1977, Vol. 13, pp. 1257–1270. Pergamon Press. Printed in Great Britain

COLLAPSE OF CYLINDRICAL, ELASTIC TUBES UNDER COMBINED BENDING, PRESSURE AND AXIAL LOADS

OLE FABIAN
Department of Ocean Engineering, The Technical University of Denmark, Lyngby, Denmark

(*Received* 26 *April* 1977; *revised* 5 *July* 1977)

Abstract—A study of the non-linear pre-buckling state and the bifurcation and initial post-buckling behaviour of infinitely long, cylindrical, elastic tubes subjected to bending, pressure and axial loads is presented. The collapse behaviour is analysed by determining both the limit load and the possibility and significance of axial wrinkling of the compressed region of the shell prior to the limit load.

INTRODUCTION

The purpose of the present paper is to investigate the collapse behaviour of infinitely long, cylindrical, elastic tubes under combined bending, pressure and axial loads. Within the theory of elasticity we must expect one of two types of failure, as indicated on Fig. 1.

One type is characterized by a smooth global maximum on the load-deflection curve. Subjected to a bending moment, the cross section of the tube is flattened out. This circumferential flattening, which is also affected by the fluid pressure, causes the non-linear load-deflection relation and results in the limit load behaviour indicated by the prebuckling path. As early as 1926 Brazier[1] succeeded in determining the limit moment for an infinitely long, circular tube subjected to pure bending. Brazier derived an expression for the strain energy per unit tube length in terms of the change in axial curvature. By minimizing this expression with respect to the change in curvature the limit moment is obtained. A more general formulation of the problem is given by Reissner[2], who deals with the case of thin-walled, cylindrical tubes of arbitrary cross section subjected to pure bending in two directions.

The other type of failure is known as a bifurcation phenomenon, and possibly, in this case, it occurs before the limit load is reached. When the load ψ exceeds the critical bifurcation load ψ_c, the compressed region of the bent tube wrinkles axially.

Bifurcation buckling of oval cylindrical shells possessing a linear pre-buckling state (neglected pre-buckling deformations) has been examined by a number of investigators[3, 5, 6]. Hutchinson[3] applies the general post-buckling theory of Koiter[4] to the case of pure axial compression and finds the initial post-buckling behaviour always to be unstable. For combined bending and axial loads Kempner and Chen[5] show that, for this case, too, the initial post-buckling behaviour is unstable. For the advanced post-buckling behaviour, however, it is shown by Kempner and Chen[6] that oval shells are able to carry axial loads above the bifurcation load, provided that the ovality is sufficiently large. The knowledge of this behaviour of oval, cylindrical shells under various loads is important because we may expect a comparable behaviour in the present problem, particularly for circular tubes.

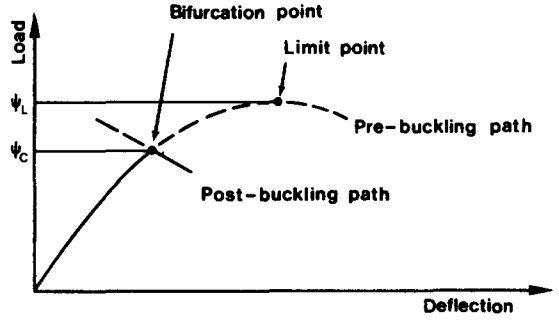

Fig. 1. General load-deflection curve.

Stephens, Starnes and Almroth[7] use a finite difference programme (STAGS) to analyse the two modes of failure for circular, cylindrical, thin-walled shells of finite length under combined bending and pressure loads. For the length-radius ratio equal to 20, this analysis shows that the collapse is caused by Brazier flattening for large external pressure and by short-wave axial buckling for large internal pressure.

The present paper is divided into three main sections. In the first section the non-linear pre-buckling state is analysed. The second section deals with the bifurcation problem and the initial post-buckling behaviour. In the last section, some numerical results are presented and discussed.

1. PRE-BUCKLING ANALYSIS

In this section, the non-linear pre-buckling state of infinitely long, cylindrical, elastic tubes subjected to bending, pressure and axial loads is analysed. The present theory approaches the theory of Reissner[2] for the case of pure bending.

Kinematic relations

We restrict ourselves to consider bending in a plane only and we must thus, in general, require that the cross section of the tube is symmetrical with respect to the plane of bending and that the moment vector is perpendicular to this plane.

When the initially straight tube is subjected to combined loads, for which the bending moment does not vanish, it deforms into a toroidal shape. Referring to the middle surface of the tube, the flattened cross section is given by the cartesian coordinates $z(s)$ and $y(s)$, where s is the circumferential arc length measured along the undeformed middle surface.

Because the tube is infinitely long it deforms into an infinite number of coincident toroids. The present theory is derived by considering a single of these toroids. We place the origin of the z–y coordinate system at the centre of this toroid and oriente the coordinate axes as shown in Fig. 2.

Due to the symmetry of the problem we need only consider the half cross section defined by $s_1 \leq s \leq s_2$. The axial fibre located at (z, y) forms a circular ring with circumferential length $l^* = 2\pi z$. With the initial length of this fibre l, the axial strain of the fibre becomes

$$\epsilon_x = \frac{l^* - l}{l} = \frac{z}{\left(\frac{l}{2\pi}\right)} - 1. \tag{1.1a}$$

For pure bending the quantity $l/2\pi$ equals the radius of curvature of the current centroid line of the tube. It turns out that the analysis is simplified by specifying the parameter $R = l/2\pi$ instead of the bending moment. Once the pre-buckling state has been determined it is easy to calculate the resulting bending moment. Another advantage in specifying the parameter R is that we are always sure of finding an equilibrium state; otherwise, a bending moment above the limit moment could be specified. Thus the axial strain of the middle surface is given by

$$\epsilon_x = \frac{z}{R} - 1. \tag{1.1b}$$

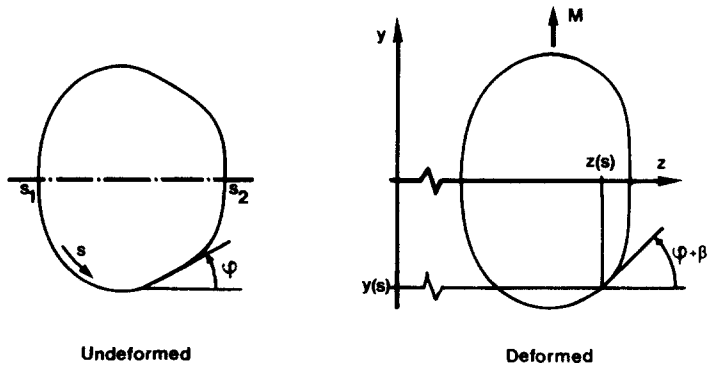

Fig. 2. Deformation of middle surface.

The angular and the circumferential strain of the middle surface, $\beta(s)$ and $\epsilon_s(s)$, respectively, are also introduced. From Fig. 2 we derive the following useful relations for the deformed middle surface

$$\frac{dz}{ds} = (1+\epsilon_s)\cos(\varphi+\beta) \tag{1.2}$$

$$\frac{dy}{ds} = (1+\epsilon_s)\sin(\varphi+\beta) \tag{1.3}$$

where $\varphi = \varphi(s)$ is an angle given by the geometry of the undeformed cross section

Equilibrium equations

The governing equilibrium equations are derived by means of the principle of minimum potential energy. For given values of the parameter R, the fluid pressure p and the additional axial force N, we start by deriving the expressions for the elastic strain energy and the potential of the applied loads.

Elastic strain energy. For thin-walled tubes the middle surface strains ϵ_x and ϵ_s are related to the membrane stresses $\bar{N}_{xx}(s)$ and $\bar{N}_{ss}(s)$ by the plane stress condition

$$\bar{N}_{xx} = \frac{Eh}{1-\nu^2}\{\epsilon_x + \nu\epsilon_s\} \tag{1.4}$$

$$\bar{N}_{ss} = \frac{Eh}{1-\nu^2}\{\epsilon_s + \nu\epsilon_x\} \tag{1.5}$$

where E, ν and $h = h(s)$ are Young's modulus, Poisson's ratio and the shell thickness, respectively. The shear strain is assumed to be zero. With these constitutive equations the expression for the elastic strain energy, which is derived in Appendix A, becomes

$$\pi_e = 2\int_{s_1}^{s_2}\left\{\frac{Eh}{1-\nu^2}\left(\frac{1}{2}\epsilon_x^2 + \frac{1}{2}\epsilon_s^2 + \nu\epsilon_x\epsilon_s\right)\right\}ds + 2\int_{s_1}^{s_2}\left\{\frac{1}{2}D\left(\frac{d\beta}{ds}\right)^2\right\}ds \tag{1.6}$$

where $D = Eh^3/12(1-\nu^2)$ is the bending stiffness of the shell. The two terms in (1.6) represent the membrane strain energy and the bending strain energy, respectively.

Potential energy of the applied loads. Because we have fixed the value of the parameter R, only the pressure and the axial loads contribute to this potential. Again, we consider a complete toroid. The volume of this toroid is given by

$$V_1 = 2\pi\int_{s_1}^{s_2}\left\{z^2\frac{dy}{ds}\right\}ds. \tag{1.7}$$

Remembering that the initial tube length of this toroid is $l = 2\pi R$ the potential energy of the hydrostatic pressure p for a unit tube length becomes

$$\begin{aligned}\pi_p &= -\left(\frac{pV_1}{2\pi R} - pV_0\right)\\ &= -\frac{p}{R}\int_{s_1}^{s_2}\left\{z^2\frac{dy}{ds}\right\}ds + pV_0\end{aligned} \tag{1.8}$$

where V_0 is the initial volume for a unit tube length. By substituting (1.1b) and (1.3) into (1.8), we obtain

$$\pi_p = -pR\int_{s_1}^{s_2}\{(1+\epsilon_x)^2(1+\epsilon_s)\sin(\varphi+\beta)\}ds + pV_0. \tag{1.9}$$

The additional, axial force N is applied at the current centroid of the cross section located at

$$z_e = 2\int_{s_1}^{s_2}\{zh\}ds \Big/ 2\int_{s_1}^{s_2} h\,ds = \frac{2}{A}\int_{s_1}^{s_2}\{zh\}ds \tag{1.10}$$

where A is the material area of the cross section.

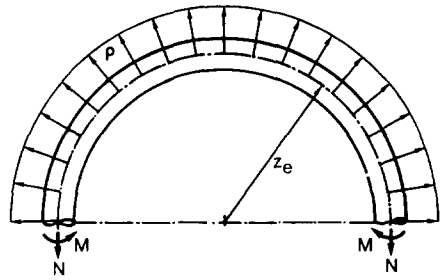

Fig. 3. Axial load and reaction.

In general the tube is not in equilibrium unless the axial force N is balanced by reactions perpendicular to the bent axis shown on Fig. 3.

Equating the reaction to the line-load (body force) per unit length

$$\rho = \frac{N}{R} \tag{1.11}$$

the potential energy for a unit tube length becomes

$$\pi_N = -(z_e - R)\rho. \tag{1.12}$$

Inserting (1.16), (1.10) and (1.11) into (1.12), we finally get

$$\pi_N = -\frac{2N}{A}\int_{s_1}^{s_2}\{h(1+\epsilon_x)\}\,\mathrm{d}s + N. \tag{1.13}$$

Equilibrium. The governing shell equations are derived by minimizing the total potential energy of the system

$$\begin{aligned}\pi &= \tau_e + \pi_p + \tau_N \\ &= \pi(\epsilon_x, \epsilon_s, \beta)\end{aligned} \tag{1.14}$$

under the constraining conditions (1.2) and (1.3). By use of (1.1b) the condition (1.2) takes the form

$$\frac{\mathrm{d}\epsilon_x}{\mathrm{d}s} - \frac{1}{R}(1+\epsilon_s)\cos(\varphi+\beta) = 0. \tag{1.15}$$

The other constraining condition (1.3) is less restrictive. This constraint only has to ensure that the boundary conditions $y(s_1) = y(s_2)$ are satisfied,

$$\int_{s_1}^{s_2}\{(1+\epsilon_s)\sin(\varphi+\beta)\}\,\mathrm{d}s = 0. \tag{1.16}$$

The ordinary and isoperimetric constraints, (1.15) and (1.16), respectively, are introduced into the minimization of (1.14) by means of the Lagrange multipliers $F(s)$ and G, the latter being a constant. The constrained minimization of the total potential energy implies the variational equation

$$\begin{aligned}\delta\int_{s_1}^{s_2}\Big\{&\frac{Eh}{1-\nu^2}\Big(\frac{1}{2}\epsilon_x^2 + \frac{1}{2}\epsilon_s^2 + \nu\epsilon_x\epsilon_s\Big) + \frac{1}{2}D\Big(\frac{\mathrm{d}\beta}{\mathrm{d}s}\Big)^2 - \frac{pR}{2}(1+\epsilon_x)^2(1+\epsilon_s)\sin(\varphi+\beta) - \frac{N}{A}h(1+\epsilon_x) \\ &+ F\Big[\frac{\mathrm{d}\epsilon_x}{\mathrm{d}s} - \frac{1}{R}(1+\epsilon_s)\cos(\varphi+\beta)\Big] + G[(1+\epsilon_s)\sin(\varphi+\beta)]\Big\}\,\mathrm{d}s = 0.\end{aligned} \tag{1.17}$$

Performing the variation with respect to ϵ_x, ϵ_s, β and F results in the 4 Eulerian equations

$$\frac{Eh}{1-\nu^2}(\epsilon_x+\nu\epsilon_s)-pR(1+\epsilon_x)(1+\epsilon_s)\sin(\varphi+\beta)-\frac{Nh}{A}-\frac{dF}{ds}=0 \tag{1.18a}$$

$$\frac{Eh}{1-\nu^2}(\epsilon_s+\nu\epsilon_x)-\frac{pR}{2}(1+\epsilon_x)^2\sin(\varphi+\beta)-\frac{F}{R}\cos(\varphi+\beta)+G\sin(\varphi+\beta)=0 \tag{1.18b}$$

$$-\frac{d}{ds}\left(D\frac{d\beta}{ds}\right)-\frac{pR}{2}(1+\epsilon_x)^2(1+\epsilon_s)\cos(\varphi+\beta)+\frac{F}{R}(1+\epsilon_s)\sin(\varphi+\beta)+G(1+\epsilon_s)\cos(\varphi+\beta)=0 \tag{1.18c}$$

$$\frac{d\epsilon_x}{ds}-\frac{1}{R}(1+\epsilon_s)\cos(\varphi+\beta)=0 \tag{1.18d}$$

and in the natural boundary conditions

$$\beta(s_1)=\beta(s_2)=0 \tag{1.19a}$$

$$F(s_1)=F(s_2)=0. \tag{1.19b}$$

The remaining boundary conditions are given by symmetry conditions. The integral condition (1.16) is satisfied by adjusting G.

The 4 non-linear simultaneous equations (1.18), one of which is algebraic, and the boundary conditions constitute the boundary value problem sought.

Once this problem has been solved, the bending moment is calculated by the formula

$$M=2\int_{s_1}^{s_2}\{\bar{N}_{xx}(z-z_e)\}\,ds. \tag{1.20}$$

For use in the post-buckling analysis we also introduce the principal radii of curvature of the shell. The circumferential radius of curvature is given by (Appendix A, eqn (A3)).

$$R_s(s)=\frac{1+\epsilon_s}{\frac{d\varphi}{ds}+\frac{d\beta}{ds}}. \tag{1.21}$$

The expression for the axial radius of curvature becomes

$$R_x(s)=\frac{z}{\sin(\varphi+\beta)}. \tag{1.22}$$

Circular cross sections

Let us consider tubes of circular cross section and constant values of h, E and ν. In this case it is appropriate to non-dimensionalize the boundary value problem. The middle surface coordinates in the axial and the circumferential direction, x and s respectively, are normalized by the radius of the cross section a.

$$\xi=\frac{s}{a}, \qquad -\frac{\pi}{2}\le\xi\le\frac{\pi}{2} \tag{1.23a}$$

$$\eta=\frac{x}{a}. \tag{1.23b}$$

The polar angle ξ equals φ. Furthermore, let us introduce for the loads

$$\alpha=\frac{a}{R}q_0^2 \tag{1.24a}$$

$$m = \frac{M}{\pi a\sqrt{(EhD)}} \tag{1.24b}$$

$$\gamma = p\left(\frac{a}{h}\right)\frac{q_0^4}{E} \tag{1.24c}$$

$$n = \frac{N}{2\pi ahE} \tag{1.24d}$$

and for the variables

$$f = \frac{F}{aEh} \tag{1.24e}$$

$$g = \frac{G}{Eh}\,(= \text{constant}) \tag{1.24f}$$

$$N_{xx} = \frac{q_0^2 a}{Eh^2}\bar{N}_{xx} \tag{1.24g}$$

$$N_{ss} = \frac{q_0^2 a}{Eh^2}\bar{N}_{ss} \tag{1.24h}$$

$$r_x = \frac{R_x}{a} \tag{1.24i}$$

$$r_s = \frac{R_s}{a} \tag{1.24j}$$

where $q_0^2 = [12(1-\nu^2)]^{1/2}a/h$. The boundary value problem now takes the form

$$\frac{1}{1-\nu^2}[\epsilon_x + \nu\epsilon_s] - \frac{\gamma}{\alpha q_0^2}(1+\epsilon_x)(1+\epsilon_s)\sin(\xi+\beta) - n - f' = 0 \tag{1.25a}$$

$$\frac{1}{1-\nu^2}[\epsilon_s + \nu\epsilon_x] - \frac{\gamma}{2\alpha q_0^2}(1+\epsilon_x)^2\sin(\xi+\beta) - \frac{\alpha}{q_0^2}f\cos(\xi+\beta) + g\sin(\xi+\beta) = 0 \tag{1.25b}$$

$$-\frac{1}{q_0^4}\beta'' - \frac{\gamma}{2\alpha q_0^2}(1+\epsilon_x)^2(1+\epsilon_s)\cos(\xi+\beta) + \\ + \frac{\alpha}{q_0^2}f(1+\epsilon_s)\sin(\xi+\beta) + g(1+\epsilon_s)\cos(\xi+\beta) = 0 \tag{1.25c}$$

$$\epsilon_x' - \frac{\alpha}{q_0^2}(1+\epsilon_s)\cos(\xi+\beta) = 0 \tag{1.25d}$$

where $(\,)'$ denotes differentiation with respect to ξ. The isoperimetric condition and the boundary conditions become

$$\int_{-\pi/2}^{\pi/2}\{(1+\epsilon_s)\sin(\xi+\beta)\}\,d\xi) = 0 \tag{1.26}$$

$$\beta\left(-\frac{\pi}{2}\right) = \beta\left(\frac{\pi}{2}\right) = 0 \tag{1.27a}$$

$$f\left(-\frac{\pi}{2}\right) = f\left(\frac{\pi}{2}\right) = 0. \tag{1.27b}$$

Numerical solution

The non-linear boundary value problem (1.25)–(1.27) is solved by means of Newton's method, as described by Thurston[8] for pure bending of tubes.

Starting with an approximate solution, this iterative method is based on solving a series of linearized boundary value problems, each step improving the solution. The linear boundary value problem at each step is solved by the finite-difference technique.

2. BUCKLING ANALYSIS

The buckling analysis presented in this section follows the approach taken by Hutchinson[3], who applied the initial post-buckling theory[4] to oval, cylindrical shells under axial compression.

Shallow shell

At the critical load level the bent tube bifurcates into a state characterized by axial wrinkling of the region of maximum compression. Prior to this bifurcation, the deformed tube has a toroidal shape, which is defined by the principal radii of curvature $r_s(\xi)$ and $r_x(\xi)$ and by the principal membrane stresses $N_{ss}(\xi)$ and $N_{xx}(\xi)$. These quantities are known from the pre-buckling analysis presented in the previous section.

The bifurcation and the initial post-buckling behaviour of this stressed toroidal shell are analysed by means of the Donnell–Mushtari–Vlasov shallow shell equations. In non-dimensional form, these non-linear equations are given by

$$\nabla^4 W + \frac{q_0^2}{r_s} F'' + \frac{q_0^2}{r_x} F^{\cdot\cdot} - 2c\{F^{\cdot\cdot} W'' + F'' W^{\cdot\cdot} - 2F'^{\cdot} W'^{\cdot}\} - \frac{\gamma}{2c} = 0 \tag{2.1}$$

$$\nabla^4 F - \frac{q_0^2}{r_s} W'' - \frac{q_0^2}{r_x} W^{\cdot\cdot} - 2c\{- W'' W^{\cdot\cdot} + (W'^{\cdot})^2\} = 0 \tag{2.2}$$

where the normal displacement $\bar{W}$ is normalized by the wall thickness, $W = \bar{W}/h$. The non-dimensional stress function is related to the non-dimensional membrane stresses by $F^{\cdot\cdot} = N_{xx}$, $F'' = N_{ss}$ and $F'^{\cdot} = -N_{xs}$ where $(\,)^{\cdot} = (\,)_{,\xi}$ and $(\,)' = (\,)_{,\eta}$. Furthermore,

$$\nabla^4(\,) = (\,)'''' + 2(\,)''^{\cdot\cdot} + (\,)^{\cdot\cdot\cdot\cdot} \qquad \text{and} \qquad c = [3(1-\nu^2)]^{1/2}.$$

Buckling equations

In order to determine the bifurcation load and the initial post-buckling behaviour we substitute the following perturbation expansions

$$W = \epsilon \overset{1}{W} + \epsilon^2 \overset{2}{W} + \cdots \tag{2.3}$$

$$F = \overset{0}{F} + \epsilon \overset{1}{F} + \epsilon^2 \overset{2}{F} + \cdots \tag{2.4}$$

into the governing eqns (2.1) and (2.2). The small parameter ϵ is here selected as the amplitude of the normal displacement in the bifurcation mode $\overset{1}{W}$, i.e. $\overset{1}{W}$ is normalized such that $\max|\overset{1}{W}| = 1$. The pre-buckling stress function is given by

$$\overset{0}{F}^{\cdot\cdot} = \overset{0}{N}_{xx}; \qquad \overset{0}{F}'' = \overset{0}{N}_{ss}; \qquad \overset{0}{F}'^{\cdot} = 0. \tag{2.5}$$

For a fixed ratio between the load components m, γ and n, the load level can be expressed by a single parameter ψ. This parameter, too, is expanded around the bifurcation point

$$\psi = \psi_c(1 + a\epsilon + b\epsilon^2 + \cdots) \tag{2.6}$$

where ψ_c is the bifurcation load. The initial post-buckling coefficients a and b are to be calculated in the analysis.

By assuming that the governing equations are valid for all ϵ, the coefficients of $\epsilon^1, \epsilon^2 \ldots$ must vanish. This gives a set of first order equations:

$$\nabla^4 \overset{1}{W} + \frac{q_0^2}{r_s} \overset{1}{F}'' + \frac{q_0^2}{r_x} \overset{1}{F}^{\cdot\cdot} - 2c\overset{0}{N}_{ss} \overset{1}{W}^{\cdot\cdot} - 2c\overset{0}{N}_{xx} \overset{1}{W}'' = 0 \tag{2.7}$$

$$\nabla^4 \overset{1}{F} - \frac{q_0^2}{r_x} \overset{1}{W}'' - \frac{q_0^2}{r_x} \overset{1}{W}'' = 0 \tag{2.8}$$

which constitutes an eigenvalue problem determining the bifurcation load ψ_c. The second-order buckling equations take the form

$$\nabla^4 \overset{2}{W} + \frac{q_0^2}{r_s} \overset{2}{F}'' + \frac{q_0^2}{r_x} \overset{2}{F}'' - 2c\overset{0}{N}_{ss} \overset{2}{W}'' - 2c\overset{0}{N}_{xx} \overset{2}{W}'' = 2c\{\overset{1}{F}'' \overset{1}{W}'' + \overset{1}{F}'' \overset{1}{W}'' - 2\overset{1}{F}'' \overset{1}{W}''\} \tag{2.9}$$

$$\nabla^4 \overset{2}{F} - \frac{q_0^2}{r_s} \overset{2}{W}'' - \frac{q_0^2}{r_x} \overset{2}{W}'' = 2c\{-\overset{1}{W}'' \overset{1}{W}'' + (\overset{1}{W}'')^2\}. \tag{2.10}$$

The boundary conditions for these two problems are obtained by seeking solutions which are periodical in the axial direction and symmetrical or asymmetrical with respect to the plane of bending in the circumferential direction.

By selecting an axially periodical solution the initial post-buckling coefficient a must vanish; otherwise, the post-buckling behaviour depends on the sign of the buckling mode. When the coefficient a vanishes, it appears from (2.6) that the stability of the equilibrium state at the bifurcation point is determined by the sign of the initial post-buckling coefficient b, i.e. the equilibrium state is unstable for negative values of b.

For the case of a non-linear pre-buckling state, Fitch[9] gives the following expression for b:

$$b = \frac{N_b}{D} \tag{2.11a}$$

where

$$N_b = -2\int_A \{\overset{1}{F}'' \overset{1}{W}' \overset{2}{W}' + \overset{1}{F}'' \overset{1}{W}' \overset{2}{W}' - \overset{1}{F}'' (\overset{1}{W}' \overset{2}{W}' + \overset{1}{W}' \overset{2}{W}')\}\, dA$$

$$- \int_A \{\overset{2}{F}'' (\overset{1}{W}')^2 + \overset{2}{F}'' (\overset{1}{W}')^2 + 2\overset{2}{F}'' (\overset{1}{W}' \overset{1}{W}')\}\, dA \tag{2.11b}$$

and

$$D = \psi_c \int_A \{(\partial \overset{0}{N}_{ss}/\partial\psi)_c (\overset{1}{W}')^2 + (\partial \overset{0}{N}_{xx}/\partial\psi)_c (\overset{1}{W}')^2 + 2(\partial \overset{0}{W}'/\partial\psi)_c (\overset{1}{F}'' \overset{1}{W}' + \overset{1}{F}'' \overset{1}{W}')\}\, dA. \tag{2.11c}$$

Here $(\partial \overset{0}{W}/\partial\psi)_c$ is determined by the pre-buckling solution presented in Section 1 by considering the geometry of the tube cross section just above and below ψ_c.

In the case of an actual tube, however, even small geometrical imperfections may greatly reduce the buckling load. The initial post-buckling theory predicts that the tube will be imperfection-sensitive, if the initial post-buckling behaviour is unstable, and vice versa. An asymptotically valid relation for this buckling load reduction takes the form

$$\left(1 - \frac{\psi_s}{\psi_c}\right)^{3/2} = \frac{3\sqrt{3}}{2} |\bar{\epsilon}| \sqrt{(-b\rho^2)} \left(\frac{\psi_s}{\psi_c}\right), \qquad b < 0 \tag{2.12}$$

where ψ_s is the buckling load for a geometry with an imperfection in the shape of $\overset{1}{W}$ and of amplitude $\bar{\epsilon}$. The coefficient ρ equals 1 for linear pre-buckling, but for the non-linear pre-buckling Fitch[9] gives the following expression

$$\rho = \frac{N_\rho}{D}. \qquad D \text{ given by eqn (2.11c)} \tag{2.13a}$$

$$N_\rho = \int_A \{\overset{0}{N}_{ss} (\overset{1}{W}')^2 + \overset{0}{N}_{xx} (\overset{1}{W}')^2\}\, dA. \tag{2.13b}$$

Numerical solution

The partial differential equations (2.7) and (2.8) separate into ordinary differential equations if we assume the solution to be of the form

$$\overset{1}{W} = w_1(\xi)\cos\lambda\eta \tag{2.14}$$

$$\overset{1}{F} = f_1(\xi)\cos\lambda\eta \tag{2.15}$$

where λ is the axial wave number. Then (2.7) and (2.8) are reduced to

$$w_1'''' + (-\lambda^2 - 2c\overset{0}{N}_{ss})w_1'' + (\lambda^4 + 2c\lambda^2\overset{0}{N}_{xx})w_1 + \frac{q_0^2}{r_x}f_1'' - \frac{\lambda^2 q_0^2}{r_s}f_1 = 0 \tag{2.16}$$

$$f_1'''' - 2\lambda^2 f_1'' + \lambda^4 f_1 - \frac{q_0^2}{r_x}w_1'' + \frac{\lambda^2 q_0^2}{r_s}w_1 = 0. \tag{2.17}$$

With these solutions (2.14)–(2.15) for $\overset{1}{W}$ and $\overset{1}{F}$, the right hand sides of the second-order eqns (2.9) and (2.10) are either independent of η or vary as $\cos 2\lambda\eta$. Therefore $\overset{2}{W}$ and $\overset{2}{F}$ are sought as

$$\overset{2}{W} = c[w_\alpha(\xi) + w_\beta(\xi)\cos 2\lambda\eta] \tag{2.18}$$

$$\overset{2}{F} = c[f_\alpha(\xi) + f_\beta(\xi)\cos 2\lambda\eta]. \tag{2.19}$$

These solutions ensure the orthogonality (i.e. the uniqueness) of the expansions (2.3) and (2.4). Thus (2.9) and (2.10) reduce to

$$w_\alpha'''' + \frac{q_0^2}{r_x}f_\alpha'' - 2c\overset{0}{N}_{ss}w_\alpha'' = -\lambda^2(f_1 w_1)'' \tag{2.20}$$

$$f_\alpha'''' - \frac{q_0^2}{r_x}w_\alpha'' = \frac{1}{2}\lambda^2(w_1^2)'' \tag{2.21}$$

and

$$w_\beta'''' + (-8\lambda^2 - 2c\overset{0}{N}_{ss})w_\beta'' + (16\lambda^4 + 8c\lambda^2\overset{0}{N}_{xx})w_\beta + \frac{q_0^2}{r_x}f_\beta'' - \frac{4\lambda^2 q^2}{r_s}f_\beta$$
$$= -\lambda^2\{f_1 w_1'' + f_1'' w_1 - 2f_1' w_1'\} \tag{2.22}$$

$$f_\beta'''' - 8\lambda^2 f_\beta'' + 16\lambda^4 f_\beta + \frac{4\lambda^2 q_0^2}{r_s}w_\beta = \lambda^2\{w_1'' w_1 - (w')^2\}. \tag{2.23}$$

The possibility of an asymmetrical buckling pattern is excluded in the following as it turns out that the bifurcation load is smallest for the buckling pattern that is symmetrical with respect to the plane of bending.

The boundary conditions describing this symmetry are

$$w_i''' = w_i' = f_i''' = f_i' = 0, \qquad i = 1, \alpha, \beta, \qquad \xi = \pm\frac{\pi}{2}. \tag{2.24}$$

This completes the formulation of the eigenvalue problem and the two second order boundary value problems.

The eigenvalue problem is solved by the finite-difference technique. The bifurcation load ψ_c is found as the smallest value of ψ that makes the determinant vanish for the corresponding system of algebraic equations. The axial wave number λ is chosen so that ψ_c attains a

minimum. When the classical bifurcation mode (w_1, f_1) is calculated we solve (2.20)–(2.23) for (w_α, f_α)† and (w_β, f_β). The finite-difference technique is used in these cases, too. Finally, we calculate the initial post-buckling coefficient b. The integration in the axial direction is performed analytically, while a numerical procedure is used for integration in the circumferential direction.

3. RESULTS

In this section the results of the numerical analysis are presented. The parameters to be varied in this analysis are the radius-thickness ratio of the tube a/h, Poisson's ratio ν and the loads m, γ and n.

It is found that the pre-buckling shape of the cross-section is almost independent of an axial tensile load, the membrane stresses are superposed by a contribution from this load, only. Thus the axial load governs the location of the bifurcation point and may prevent bifurcation buckling prior to the limit moment. This significance of the axial load, however, is rather tedious, so in the following we select a load combination for which $m = \psi$, $\gamma =$ constant and $n = 0$. That is, the initial post-buckling analysis describes the moment-curvature relation for fixed pressure and zero axial load. For ν we use the value 1/3.

Figure 4 shows the pre-buckling behaviour and the bifurcation point for different values of the pressure. The bifurcation pressure for pure pressure load corresponds to $\gamma_c = -3$.

As indicated in this figure, the limit point is not found for large external pressure, because the calculations are terminated when the opposite walls of the tube start overlapping $(z(-\pi/2) \geq z(+\pi/2))$. For the moment approaching zero, this overlapping is found to start at $\gamma \simeq -5.5$.‡ In this representation of the results it is found that the pre-buckling behaviour is not significantly influenced by the ratio a/h.

The location of the bifurcation point, however, varies according to the ratio a/h and is shown for $a/h = 60$ in Fig. 4. It is found that the bifurcation point is bounded by the limit point as the ratio a/h becomes small. For large values of the ratio a/h the bifurcation point approaches the engineering approximation that bifurcation occurs when the maximum, compressive stress reaches the critical stress for a uniformly axially loaded, circular cylinder with radius to thickness equal to $R_s(-\pi/2)/h$. Furthermore, Fig. 4 shows that the bifurcation moment and the limit moment almost coincide for $\gamma \simeq -2$, while for internal pressure (and large external

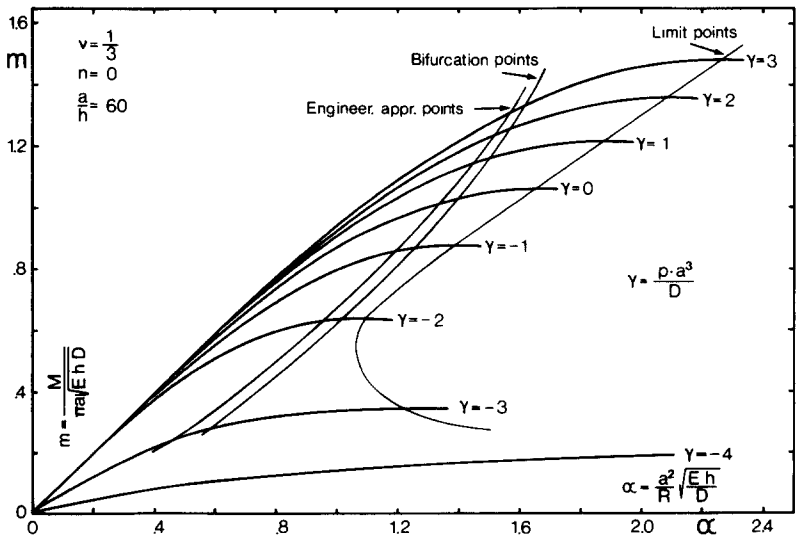

Fig. 4. Dimensionless moment-curvature relation.

†The boundary conditions (2.24) determine w_α except for an arbitrary constant. This constant is determined by the condition that the circumferential displacement must be single-valued. However, this constant is not necessary for the calculation of b.

‡For small values of the moment the corresponding ovalization of the tube can be regarded as an imperfection with respect to pure pressure load. Thus the present pre-buckling analysis includes the advanced post-buckling behaviour of an imperfect tube under pure pressure load.

pressure) the bifurcation moment is slightly below the limit load. This effect of the pressure is also found by Stephens *et al.*[7] for a tube with length-radius ratio $L/a = 20$ and with $a/h = 100$.

Figure 5 shows a comparison between the results obtained by the present approach and the empirical interaction curve given by

$$\left(\frac{M_L}{M_{L,0}}\right)^2 + \frac{p}{p_c} = 1$$

where $M_{L,0}$ is the limit moment without pressure and p_c is the bifurcation pressure. Brazier[1] found $M_{L,0} = 1.047\, ah^2E$.

Figure 6 shows the pre-buckling shapes of the initially circular cross section at the bifurcation point and at the limit point. All shapes are almost double symmetrical, only a close investigation of the coordinates indicates a small unsymmetry about the elastic axis for bending.

The corresponding dimensionless membrane stresses for zero pressure are given on Fig. 7.

Figure 8 shows the classical bifurcation mode $w_1(\xi)$ for various values of the pressure.

As we may expect, the wrinkling of the compressed region of the tube occurs more locally for a thinner or less flattened tube than for a thicker or more flattened tube. This behaviour also appears from Fig. 9, which shows the critical axial wave length $2\pi/h$.

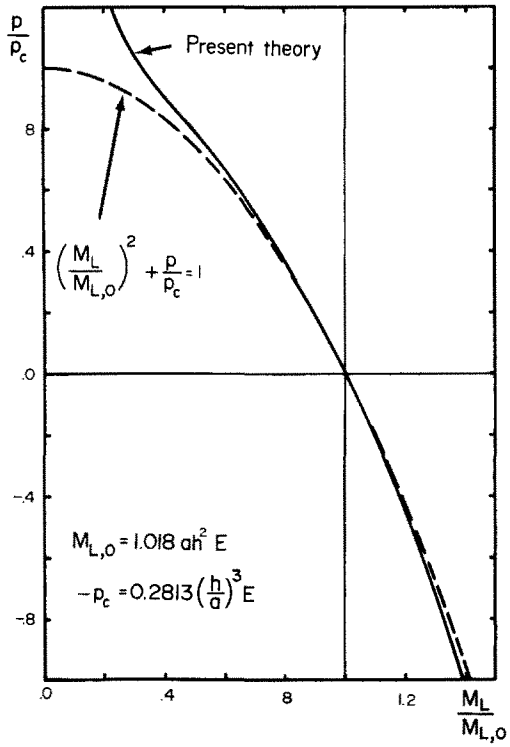

Fig. 5. Limit moment vs fluid pressure.

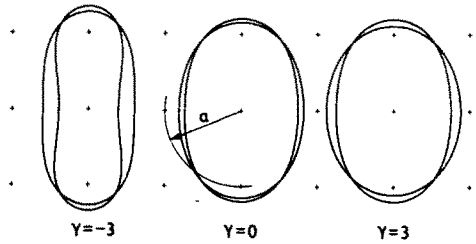

Fig. 6. Pre-buckling shapes of initial circular cross section at bifurcation point and limit (most ovalized) point.

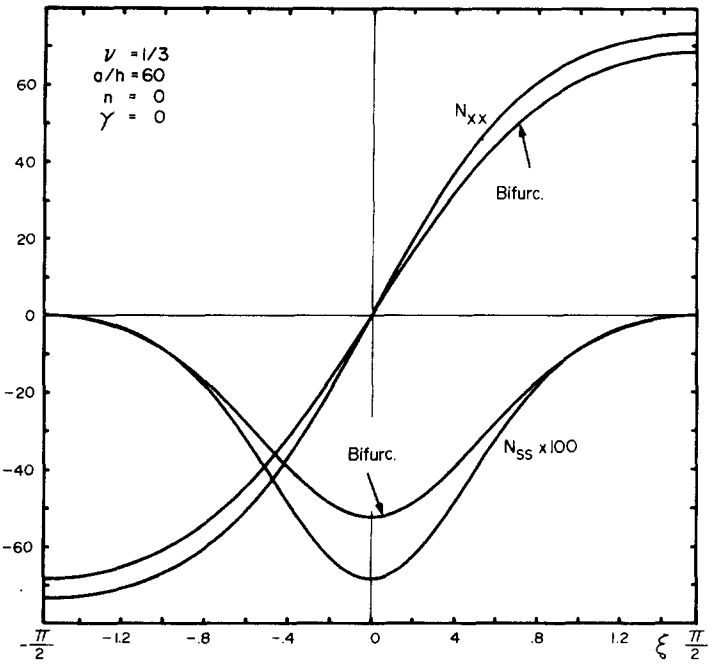

Fig. 7. Dimensionless pre-buckling membrane stresses at bifurcation and limit moment.

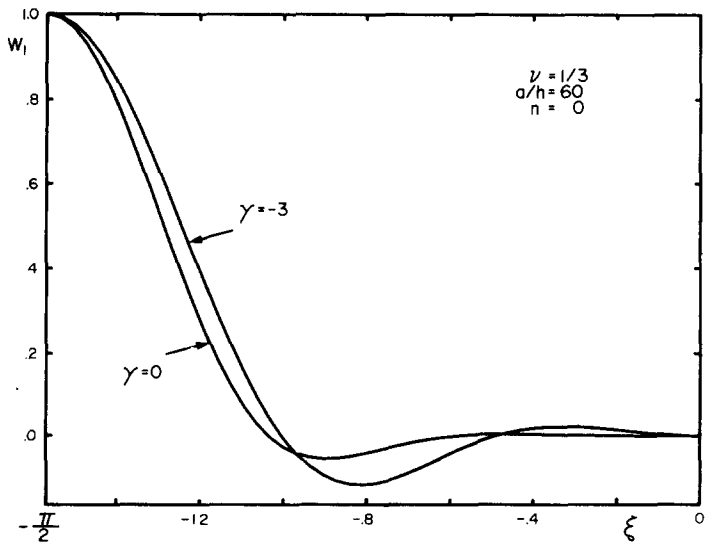

Fig. 8. Circumferential variation of classical bifurcation mode.

Finally Fig. 10 shows the initial post-buckling coefficient b and the modified coefficient $b\rho^2$. For the cases considered the equilibrium state is always found to be unstable ($b < 0$), so that the tube is sensitive to geometrical imperfections.

The behaviour shown on Fig. 10 agrees qualitatively with the results of Kempner and Chen[5] for oval, cylindrical shells under bending and axial load and assuming a linear pre-buckling state.

To determine whether the bifurcation causes collapse of the tube, however, we need an investigation of the advanced post-buckling behaviour.

CONCLUSION

The collapse behaviour of infinitely long, cylindrical tubes under bending, pressure and axial loads has been analysed. Within the law of elasticity, two modes of failure have been investigated. One mode is caused by the circumferential flattening of the tube and thus

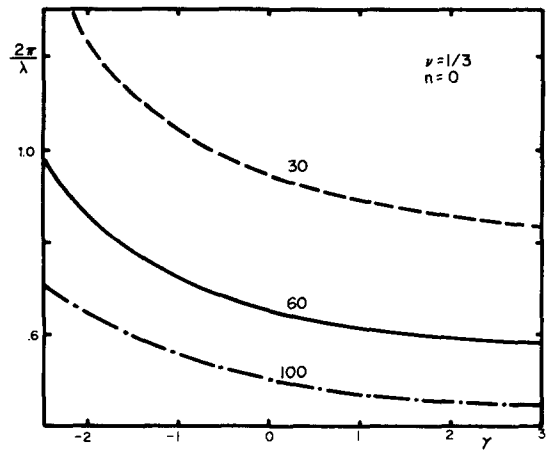

Fig. 9. Critical axial wave length vs pressure for $a/h = 30, 60, 100$.

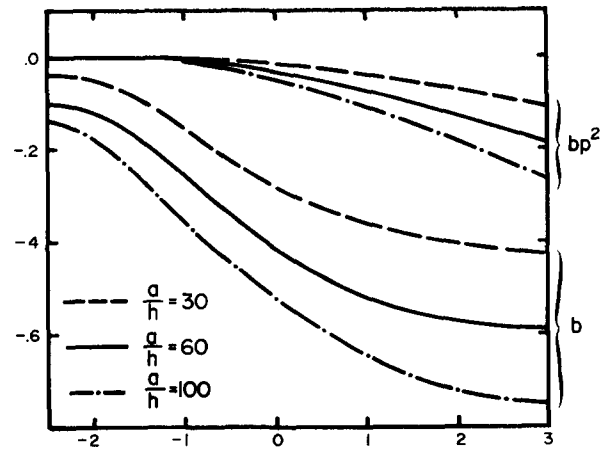

Fig. 10. Initial post-buckling coefficients vs pressure for $a/h = 30, 60, 100$.

constitutes a limit load problem. In the other mode, the compressed region of the tube wrinkles axially, i.e. bifurcation buckling occurs.

For the perfect, circular tube without axial load, the bifurcation moment and the limit moment almost coincide. The initial post-buckling behaviour is always found to be unstable, but the imperfection sensitivity is less significant for large external pressure or thick-walled tubes.

REFERENCES

1. L. G. Brazier, On the flexure of thin cylindrical shells and other sections. *Proc. Royal Soc. Series A.* **CXVI**, 104–114 (1926).
2. E. Reissner, On finite pure bending of cylindrical tubes. *Österr. Ing. Arch.* **15**, 165–172 (1961).
3. J. W. Hutchinson, Buckling and initial postbuckling behaviour of oval cylindrical shells under axial compression. *J. Appl. Mech.* (*ASME*) 66–72 (1968).
4. W. T. Koiter, Over de stabiliteit van het elastish evenwicht (On the stability of elastic equilibrium), Thesis, Delft, H. J. Paris, Amsterdam (1945). (English translation issued as NASA TT F-10, 833, 1967).
5. J. Kempner and Y.-N. Chen, Buckling and initial postbuckling of oval cylindrical shells under combined axial compression and bending. *Trans. New York Academy of Sci.* **36**, Series II, No. 2, pp. 171–191 (1974).
6. J. Kempner and Y.-N. Chem, Buckling and postbuckling of an axially compressed oval cylindrical shell. pp. 141–183, Polytechnic Institute of Brooklyn, *PIBAL Report* No. 917, (April 1966), presented at Seventy Anniversary Symposium on Shells to honor Lloyd H. Donnel.
7. W. B. Stephens, J. H. Starnes and B. O. Almroth, Collapse of long cylindrical shells under combined bending and pressure loads. *AIAA J.* **13**, 20–25 (1975).
8. G. A. Thurston, Newton's method applied to problems in nonlinear mechanics. *J. Appl. Mech.* (*ASME*) 383–388 (June 1965).
9. J. R. Fitch, The buckling and postbuckling behaviour of spherical caps under concentrated load. *Int. J. Solids Structures*, **4**, 421–446 (1968).

APPENDIX A

Elastic energy

A material point of the cross section is defined by the circumferential arc length s and the distance from the middle surface t, see Fig. A1.

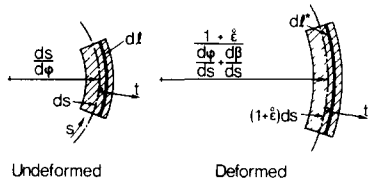

Fig. A1. Deformation of circumferential fiber.

To derive expressions for $\epsilon_x(s,t)$ and $\epsilon_s(s,t)$ we assume that normals to the middle surface remain perpendicular to this during the deformation, i.e. there is no shear deformation in the s-direction either.

The axial strain of a fibre located at (s,t) then becomes

$$\epsilon_x(s,t) = \frac{z + t\sin(\varphi+\beta)}{R} - 1$$

$$= \overset{0}{\epsilon}_x(s) + \frac{t}{R}\sin(\varphi+\beta) \tag{A1}$$

where $\overset{0}{\epsilon}_x = \epsilon_x(s,0)$ is the middle surface strain given by (1.1). This expression must be used for thick-walled tubes, whereas the last term can be omitted for moderately thin-walled tubes.

To derive an expression for $\epsilon_s(s,t)$ we start considering the curvature of the middle surface in the circumferential direction

$$\frac{1}{R_s} = \frac{\dfrac{dy}{ds}\dfrac{d^2z}{ds^2} - \dfrac{d^2y}{ds^2}\dfrac{dz}{ds}}{\left(\left(\dfrac{dy}{ds}\right)^2 + \left(\dfrac{dz}{dw}\right)^2\right)^{3/2}}. \tag{A2}$$

By substituting (1.2) and (1.3) into (A2), we get

$$\frac{1}{R_s} = \frac{\dfrac{d\varphi}{ds} + \dfrac{d\beta}{ds}}{1 + \overset{0}{\epsilon}_s} \tag{A3}$$

where $\overset{0}{\epsilon}_s = \epsilon_s(s,0)$. The undeformed length dl of a circumferential fibre segment located at (s,t) is, see Fig. A1,

$$dl = ds\left[1 + \frac{d\varphi}{ds}\cdot t\right]. \tag{A4}$$

In the deformed state, the fibre length becomes

$$dl^* = (1 + \overset{0}{\epsilon}_s)\,ds\left[1 + \frac{t}{R_s}\right] \tag{A5}$$

so for the circumferential strain we obtain

$$\epsilon_s(s,t) = \frac{dl^* - dl}{dl} = \frac{\overset{0}{\epsilon}_s + t\dfrac{d\beta}{ds}}{1 + t\dfrac{d\varphi}{ds}}. \tag{A6}$$

When t equals $h/2$, the quantity $t(d\varphi/ds)$ in the denominator of (A6) represents the local thickness-diameter ratio. For moderately thin tubes this term is dropped.

For the plane stress state without shear deformations the strain energy for unit tube length becomes

$$\pi_e = 2\int_{s_1}^{s_2}\int_{-h/2}^{h/2}\left\{\frac{1}{2}\sigma_x\epsilon_x + \frac{1}{2}\sigma_s\epsilon_s\right\} dt\,ds \tag{A7}$$

where $\sigma_x = \sigma_x(s,t)$ and $\sigma_s = \sigma_s(s,t)$ are the stresses in the two directions. Assuming the linear stress-strain relation (1.4)–(1.5) and using the expressions (A1) and (A6) we get for the thin tube

$$\pi_e = 2\int_{s_1}^{s_2}\left\{\frac{Eh}{1-\nu^2}\left(\frac{1}{2}\overset{0}{\epsilon}_x{}^2 + \frac{1}{2}\overset{0}{\epsilon}_s{}^2 + \nu\overset{0}{\epsilon}_x\overset{0}{\epsilon}_s\right)\right\} + 2\int_{s_1}^{s_2}\left\{\frac{Eh^3}{12(1-\nu^2)}\left(\frac{1}{2}\frac{d\beta}{ds}\right)\right\} ds. \tag{A8}$$

Here, the former term is recognized as the membrane strain energy, and the latter as the bending strain energy only taking the circumferential membrane bending into account.